Graphene liquid cells assembled through loop-assisted transfer method and located with correlated light-electron microscopy

Deursen, P.M.G. van; Koning, R.I.; Tudor, V.; Moradi, M.A.; Patterson, J.P.; Kros, A.; ... ; Schneider, G.F.

ADVANCED FUNCTIONAL MATERIALS
www.afm-journal.de

Graphene Liquid Cells Assembled through Loop-Assisted Transfer Method and Located with Correlated Light-Electron Microscopy

*Pauline M. G. van Deursen, Roman I. Koning, Viorica Tudor, Mohammad-Amin Moradi, Joseph P. Patterson, Alexander Kros, Nico A. J. M. Sommerdijk, Abraham J. Koster, and Grégory F. Schneider**

Graphene liquid cells (GLCs) for transmission electron microscopy (TEM) enable high-resolution, real-time imaging of dynamic processes in water. Large-scale implementation, however, is prevented by major difficulties in reproducing GLC fabrication. Here, a high-yield method is presented to fabricate GLCs under millimeter areas of continuous graphene, facilitating efficient GLC formation on a TEM grid. Additionally, GLCs are located on the grid using correlated light-electron microscopy (CLEM), which reduces beam damage by limiting electron exposure time. CLEM allows the acquisition of reliable statistics and the investigation of the most common shapes of GLCs. In particular, a novel type of liquid cell is found, formed from only a single graphene sheet, greatly simplifying the fabrication process. The methods presented in this work—particularly the reproducibility and simplicity of fabrication—will enable future application of GLCs for high-resolution dynamic imaging of biomolecular systems.

1. Introduction

Graphene liquid cells (GLCs) are femtoliter pockets of water confined between two layers of graphene. These ultrathin graphene-water structures offer a nanoscale environment for water-based processes, enabling real-time transmission electron microscopy (TEM) at room temperature. While the development of liquid cells brought about atomic resolution imaging of metallic nanoparticle growth,[1–6] visualizing processes of organic matter remains highly challenging.[7] Organic molecules, made up of low atomic number elements, are weaker electron scatterers than for instance metal atoms, yielding lower contrast in electron images. Moreover, the interaction of the electron beam with biomolecules, organic molecules, and all liquids causes radiolysis of chemical bonds in samples. The electron dose used for imaging organic materials is therefore limited, generally resulting in a low signal-to-noise ratio.[8]

Conventional, silicon-based liquid cells confine water between two SiN nanomembranes. The electron pathway through both the SiN and water induces significant electron scattering.[9,10] Graphene, on the other hand, is a single atomic layer that causes minimal background electron scattering.[11] Moreover, graphene is a thermal and electrical conductor that prevents beam-induced damage by facilitating fast energy dissipation.[12] The advantage of graphene in electron imaging of soft matter was investigated recently, revealing an order of magnitude higher spatial resolution in graphene-coated TEM specimen compared to specimen without graphene, fixated by plunge-freezing.[13]

Therefore, GLCs offer the prospect of the high-resolution, dynamic imaging of biological processes, for example protein function and lipid membrane fusion. The first GLC studies of bio-organic systems at room temperature include $SKBR_3$ breast cancer cells, the H_3N_2 influenza virus,[14,15] microtubulines[13] and polystyrene chains in water resolved at the level of individual molecules.[16]

Beyond the first successes, demonstration of reproducible data acquisition must be the next step toward application to specific case studies in life sciences. Currently, poor reproducibility of GLC fabrication methods is undoubtedly delaying this development. An important requirement of the fabrication procedure is that graphene is transferred without the use of polymer

P. M. G. van Deursen, V. Tudor, Prof. A. Kros, Dr. G. F. Schneider
Leiden Institute of Chemistry
Leiden University
Einsteinweg 55, 2333 CC Leiden, The Netherlands
E-mail: g.f.schneider@chem.leidenuniv.nl
Dr. R. I. Koning, Prof. A. J. Koster
Leiden University Medical Center
Leiden University
Einthovenweg 20, 2333 ZC Leiden, The Netherlands
Dr. M.-A. Moradi, Dr. J. P. Patterson
Laboratory of Materials and Interface Chemistry & Center of Multiscale Electron Microscopy
Department of Chemical Engineering and Chemistry, and Institute for Complex Molecular Systems
Eindhoven University of Technology
P.O. Box 513, 5600 MB Eindhoven, The Netherlands
Prof. N. A. J. M. Sommerdijk
Radboud University Medical Center
Department of Biochemistry
Radboud Institute for Molecular Life Sciences
6525 GA Nijmegen, The Netherlands
The ORCID identification number(s) for the author(s) of this article can be found under https://doi.org/10.1002/adfm.201904468.

DOI: 10.1002/adfm.201904468

support layers, as transfer polymers inevitably leave trace contaminations visible during TEM imaging.[17] A recent review lists current methods for assembling GLCs on TEM grids but falls short of giving clarity on the efficiency of each method toward GLC fabrication.[18] We include here a concise overview of common GLC assembly methods. To our knowledge the most common method comprises the sandwiching of water between two TEM grids carrying graphene on a porous support film.[19–22] As graphene is supported through the sample assembly procedure, this method has the largest chance of retaining graphene integrity, albeit at the cost of losing graphene flexibility. Another drawback lies in the double support layers that are sandwiched together, obscuring a large part of the imaging area by support material.

Other methods come down to the addition of a top graphene layer from the surface of water (or an aqueous specimen solution/dispersion) to a graphene-coated TEM grid. This assembly method can be achieved in two ways. First, the graphene layer can be scooped from below onto the grid.[14,15] This approach induces mechanical stress to the free-floating graphene layer and has to date only been demonstrated using multilayer graphene. Alternatively, the grid can be placed on top of the floating graphene layer (we shall refer to this approach as the "touch-down" method). In the touch-down method, the specimen liquid can be added as a droplet to the grid,[16,23] or be sprayed as micro-droplets onto either graphene layer. The latter approach has been shown to render large area intact graphene.[24]

We note that most often, multilayer graphene is used in these methods, because its superior stability. Both multilayer graphene or defect-free single crystals of graphene has been shown to increase success rates,[16,19] but the availability of these materials is limited. Moreover, single layer graphene is preferred over multilayer graphene, as the latter is more rigid and often contaminated by the preparation procedure in which single graphene layers are stacked using polymer transfer.

Here, we present an efficient and reproducible approach to fabricate GLCs by loop-assisted transfer (LAT) of graphene. We validate the LAT approach by comparison to two other GLC fabrication methods widely used in literature: the touch-down method and the grid sandwich method. The three methods investigated in this paper (LAT, touch-down and grid sandwich), require no lithographic substrate preparation[25] or liquid handling equipment.[26] Moreover, the methods were selected on the fact that the specimen liquid can be added as a macroscopic droplet, requiring no large volumes or micro-spraying. These choices are motivated by the conviction that accessibility of the technique is a prerequisite for widespread adaptation of GLCs in biomaterials and microbiological research, where micro- and nanofabrication are not commonplace.

To obtain a representative count of the GLCs on each grid, we employed correlated light-electron microscopy (CLEM). With a systematic comparison of fabrication methods and detailed description of GLC formation mechanisms we aim to set a standard for fabricating GLCs, paving the way to widespread implementation of GLCs in high resolution TEM imaging of room temperature specimen.

2. Results and Discussions

2.1. Low Stress Graphene Transfer

Figure 1 summarizes the procedure of graphene liquid cell fabrication. Single layer graphene was grown on a copper substrate by chemical vapor deposition. In the case of the LAT and touch-down methods, GLCs are assembled on a TEM grid coated with a porous polystyrene film that gives support to the bottom graphene sheet (Figure 1a, steps I–IV). The fabrication of the polystyrene film is described in the Methods. The pore-to-support ratio can be varied by changing fabrication parameters, with a 50:50 pore-to-support ratio representing the largest area of open space while still yielding a stable support membrane. In our experience, polystyrene-supported grid preparation has proven more reliable than direct transfer[27] onto support films attached to TEM grids. The success rate with which TEM grids are coated with polystyrene-supported graphene exceeds 98%. The high yield is attributed to the addition of the support film as flexible layer onto the graphene-copper stack, resulting in very reliable adhesion of graphene to the film.

Figure 1b, left panel, shows the method adapted in our laboratory for the transfer of the second graphene sheet: the loop assisted transfer, or LAT. A bare graphene sheet is freely floating on a water-air interface prior to transfer. Graphene is transferred using a 2 mm inner diameter metal loop carrying a droplet of water along with the floating graphene layer onto the grid (Figure 1b). As the droplet is blotted by filter paper and the grid is left to dry, the top layer comes into contact with the bottom graphene layer, forming liquid cells. This approach induces minimal stress to the graphene layer, resulting in a large area of intact graphene after transfer (Figure 1f). Drying of the last remaining water was recorded under an optical microscope (Movie S1, Supporting Information). The movie shows that a thin layer of water remains suspended in the holes of the support film, separating the two graphene layers until the very last moment, when liquid cells form. We note here that the polystyrene support film was otherwise of little influence on the formation, size or distribution of liquid cells observed in our experiments. The bottom graphene layer is a flat graphene sheet without noticeable wrinkles (Figure S2, Supporting Information). The top graphene layer is flexible at the moment of contact with the bottom layer, so that curvature and wrinkles allow for the formation of liquid cells (Figure 3b).

GLC formation efficiency was compared with two commonly reported methods of graphene liquid cell fabrication.[16,21] We quantified the total number of GLCs fabricated through each method (**Table 1**). The GLC count was obtained as described in the Methods. In our experience, the touch-down method (Figure 1c) resulted in fractured graphene patches that poorly covered the TEM grid. The second graphene layer is subject to mechanical stress during the deposition. Moreover, the interplay of surface tension between the two water phases (the droplet on the grid and the water underneath the second graphene sheet) causes local water turbulence. For these reasons, the approach yields a highly ruptured and crumbled second graphene layer, even if multilayer or monocrystalline graphene are used.[14,16,19,24] Graphene deposited by the LAT and the touch-down method onto a paper substrate reveal the difference in surface coverage between both methods (Figure 1f,g).

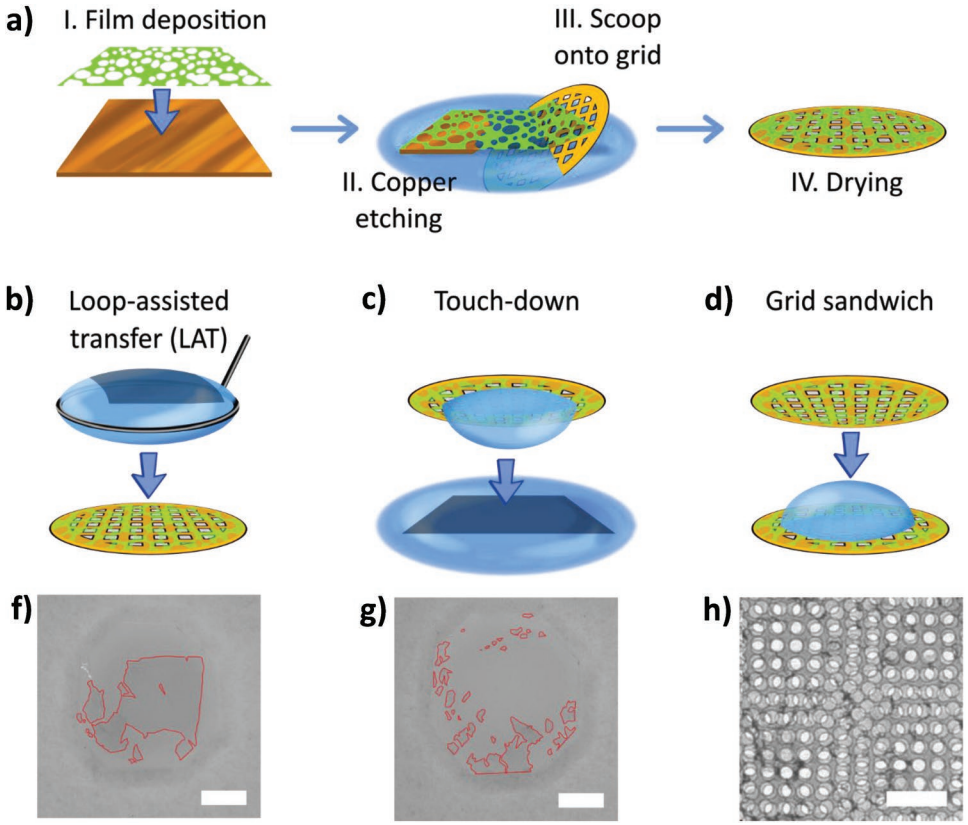

Figure 1. Comparison of loop-assisted preparation of graphene liquid cells. a) Preparation of bottom layer graphene supported by a porous polystyrene film on a TEM grid. b–d) Methods for fabricating a graphene–water–graphene stack for the formation of liquid cells: b) loop-assisted graphene transfer (LAT) of graphene onto a graphene-coated TEM grid, sandwiching water between the two graphene layers to form liquid cells. c) Fabrication of liquid cells by the touch-down method, where a graphene-coated TEM grid is placed on an unsupported graphene sheet floating on water. d) Fabrication of liquid cells by the sandwich method, where two graphene-coated TEM grids are placed on top of each other, sandwiching a droplet of water. f–h) The quality of graphene transfer by the methods described in (b)–(d). e) Optical microscopy image showing the graphene coverage on a paper background after transfer by the LAT method illustrated in (b). Red line marks the edge of the graphene sheet. Scale bar: 1 mm. f) Optical microscopy image showing the graphene coverage after transfer by the touch-down method (c). Red line marks the edge of the graphene sheet. Scale bar: 1 mm. g) Overlap of holey carbon support layers that occurs on a sample prepared by the sandwich method (d). Darker regions represent the support films that obscures most of the view, while the light holes represent the areas where only two graphene layers are in the beam path and potential graphene liquid cells can form. Scale bar: 10 µm.

Graphene absorbs too little light to be visible against the polystyrene film on a TEM grid. White paper was therefore chosen as background substrate to visualize the coverage of graphene by optical microscopy. The coverage and integrity of graphene after LAT and touch-down transfer were also investigated on a silicon oxide wafer (Figure S3, Supporting Information).

The last method omits the transfer of flexible graphene altogether: two graphene-coated TEM grids are sandwiched together with a droplet of water in between (Figure 1d).[1,21] Although the grid-sandwich method ensures mechanical support to both graphene layers, GLC formation is hampered by the loss of flexibility caused by the porous support film that rigidly suspends both graphene layers. On the six grids successfully sandwiched in our lab, a total of three liquid cells were found. Besides low GLC count, the two holey support layers overlap in random orientation, so that most of the grid area is obscured by at least one support layer (Figure 1h). GLCs that form suffer from contrast loss due to the support layer in the beam path.

Table 1. Efficiency toward GLC formation of three fabrication strategies. All liquid cells counted were confirmed by high magnification TEM imaging. The number of GLCs per grid was extrapolated taking into account the area of the grid that was investigated on each grid.

	Total GLC count	Number of grids prepared	Extrapolated number of GLCs per grid
Loop-assisted transfer (LAT)	184	21	300
"Touch-down" transfer	18	8	80
TEM grid sandwich	3	6	~1

2.2. Fluorescent Labeling for Low Dose Sample Screening

GLCs and their contents are commonly exposed to the electron beam during screening of the grid to locate GLCs. This is undesirable, as GLCs and their aqueous content are electron beam sensitive. Moreover, as liquid cells can be distributed sparsely over the grid, locating them at high magnification is a time-consuming task faced in all GLC experiments regardless of the

GLC fabrication method. Therefore we introduced a method to locate liquid cells using light microscopy, adding a low concentration of high quantum yield fluorescent dye (Atto 488, 10×10^{-6} M) to the water. **Figure 2**a shows an optical microscopy image of a TEM grid featuring fluorescent-tagged GLCs. Some background fluorescence reveals the contours of the polystyrene support film, as polystyrene weakly fluoresces in the green spectral region. Figure 2b shows an overlay of the fluorescent and electron image at low magnification of the same grid. White arrows indicate liquid cells, of which one example is shown in Figure 2c. Typical to encapsulated liquid water is the disappearance of the feature upon exposure to high electron dose (Figure 2d and Figure S4a–e, Supporting Information), and their appearance as a small dot on fluorescent image. On the other hand, dye solution can dry out on the TEM grid outside of graphene encapsulation. This resulted in large, bright spots on the fluorescent image (Figure S4f,g, Supporting Information), and TEM images revealed dry deposits of dye on these locations. This type of dried out dye deposits was therefore clearly distinguishable from dissolved dye encapsulated in GLCs. Using correlated fluorescent-electron microscopy, the whole grid can be screened at the level of individual grid squares (100×100 μm^2), allowing direct identification of GLCs on the grid.

2.3. Three Types of Graphene Liquid Cells

GLCs created by the loop-assisted fabrication method show areas of high GLC density (**Figure 3**b). To obtain a representative count of the liquid cells on a grid, an area of at least eight windows of 100×100 μm^2 was imaged on every grid throughout this study. Over 21 grids, the average GLC density extrapolated to the total grid area was 300 cells per grid—equivalent to one cells per two grid squares. The cell size distribution is presented in Figure 3a, showing that their frequency of occurrence drops with cell size. The cells size ranges up to 700 nm in lateral size, with an extremely high population at lower lateral sizes. For a pocket of water to be encapsulated, the top and bottom graphene layer must form a uninterrupted seal around the circumference of the GLC. The probability of a

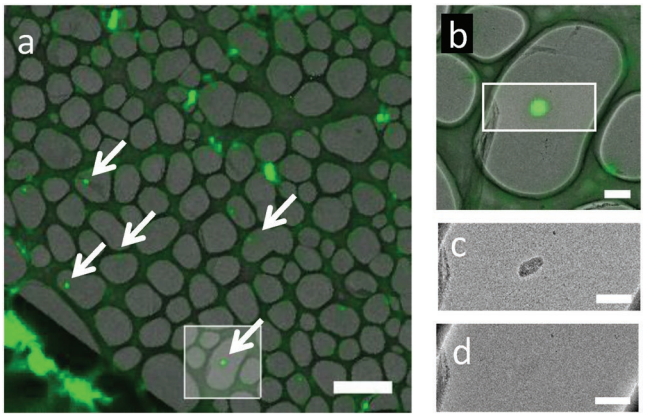

Figure 2. Correlated fluorescence-electron microscopy. a) Overlay of a fluorescent microscopy image and a low magnification TEM image, correlated in MAPS software. In view is a TEM grid featuring graphene liquid cells fabricated through the loop-assisted transfer method. White arrows indicate fluorescent dots that were confirmed to represent liquid cells by transmission electron microscopy at higher magnification as shown in b through d. Scale bar: 10 μm. b) Overlay of a fluorescent image and a high magnification electron image at of the white square in a), showing a single graphene liquid cell. Scale bar: 1 μm. c) Electron image of the area indicated by the white square in b) showing the darker contrast of a liquid cell. Scale bar: 500 nm. d) The liquid cell in (c) after exposure to the focused electron beam. The contrast has disappeared, confirming that the content of the feature was liquid. Scale bar: 500 nm.

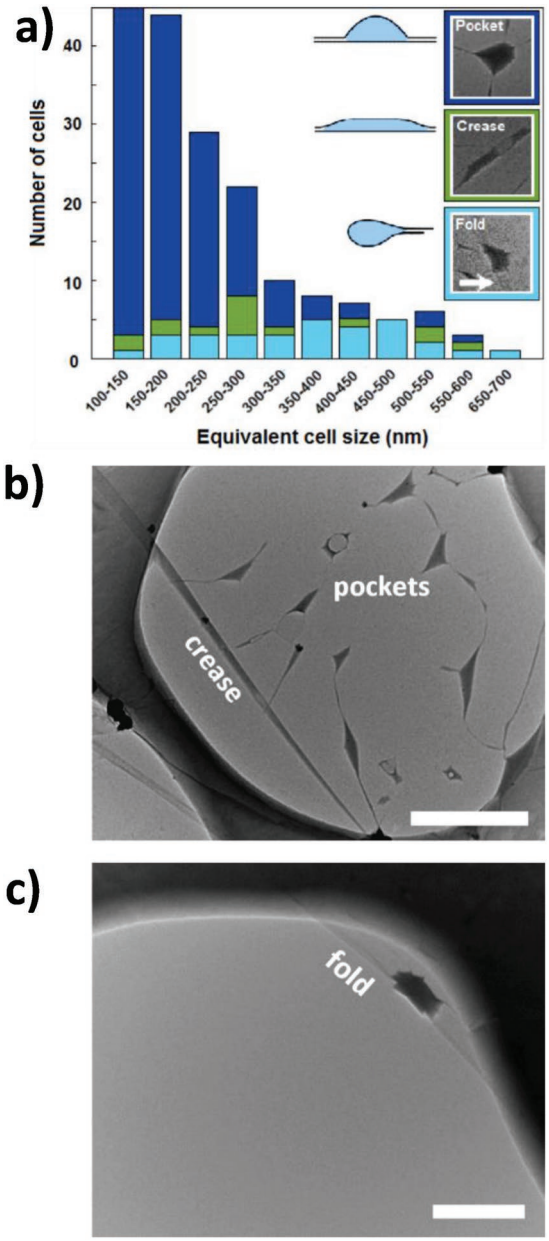

Figure 3. Three types of graphene liquid cells. a) Sum total occurrence of liquid cells sorted by type as a function of their size. The equivalent cell size is defined as the square root of the cell area. The white arrow indicates the edge of a graphene sheet where it folds back on itself. b) TEM image of a double sheet of graphene encapsulating a number of liquid cells of "pocket" and "crease" types. Scale bar: 500 nm. c) A "fold" type graphene liquid cell encapsulated in a single sheet of graphene. Scale bar: 500 nm.

leak in the seam increases with increasing cell circumference, explaining the general trend of decreasing GLC frequency with increasing size. As the bottom layer is stretched flat, the volume of a liquid cell is determined by the shape of the top graphene layer, which is flexible during the last stage of graphene deposition, when liquid cell formation occurs.

The dimensions of small liquid cells go down to the point where a liquid cell can no longer be faithfully distinguished from an irregularity in the top graphene layer (several examples can be seen in Figure 3b). Considering that liquid cells need a significant volume to be of interest in further studies, GLCs with a lateral size smaller than 200 nm^2 were disregarded in the following discussion. In total, 90 cells larger than 200 nm^2 were observed. For a more detailed understanding of the graphene sealing mechanism, we distinguished three types of liquid cells, presented in the panels of Figure 3a and in Figure 3b,c. They include: I) "pocket" cells, that are enveloped by the top graphene layer in a roughly equilateral fashion, II) "crease" cells, where water is trapped in long creases in the top layer, and III) "fold" cells, forming where a single ruptured graphene layer folds back on itself.

Pocket cells form the majority (74%) of GLCs. The flexibility of the top graphene layer plays an important role in the formation of pocket cells: to accommodate for the volume of water, the flexible top layer curves around the liquid volume, typically folding into a discrete number of corners at the GLC edge. The top middle panel in Figure 3a shows a five-cornered pocket cell. In TEM images, the relative thickness of liquid cells can be roughly estimated from the contrast of liquid cells on a single TEM image. This comparison is relative and only holds if the beam settings are equal. Therefore comparison was only made between different liquid cells that featured on the same image. It was noticed that a larger number of corners around a pocket cell generally accommodate a thicker pocket of water. Generally, pockets of liquid encapsulated by Van der Waals surfaces such as graphene show correlation between pocket size and height.[28] In our analysis, three or four-cornered cells generally appear thinner than five or more-cornered cells of the same size. The volume of a pocket cell is thus not strictly correlated to its projected size on a TEM image, as can also be seen from the GLCs presented in Figure S5 (Supporting Information). Instead, the number of corners determined the curvature of the top layer and thus the volume of a pocket GLC.

Crease type cells, formed in long folds in the top graphene layer, make up 12% of cells in the size range > 200 nm^2. The difference in structure between crease and pocket cells is highlighted in Figure 3b. As can be seen from the distribution in Figure 3a, crease cells are larger on average than pocket cells: because of the long, straight walls the top layer forms a watertight seal more easily over a greater length. However, because creases in the top graphene layer are rare, crease cells make up only a small percentage of liquid cells.

Fold cells are the third GLC type and make up 29% of the cells in the size range of interest. Fold cells form where the bottom layer of graphene is ruptured and folds back on itself (Figure 3c). The formation of fold cells occurs during the deposition of the first graphene layer on the TEM grid and was also observed on grids bearing only one graphene layer (that is, after step III in Figure 1a). Fold cells have a larger probability of encapsulating larger volumes of water and occupy the size range from 250 to 400 nm (Figure 3a). Furthermore, fold cells form on places where a single graphene layer is torn and rolls up against the polymer support layer. Since one side of a fold cell is made up of a single continuous sheet of graphene, the sealing of the top and bottom layer happens on the remaining sides of the cell, yielding a cylindrical cross-section and making them thicker on average than pocket or crease cells.

To demonstrate the efficacy of each liquid cell type toward imaging dynamic processes, we studied the formation of gold nanoparticles under electron irradiation for each cell type. For this, an aqueous solution of $HAuCl_4$ was encapsulated in GLCs and exposed to the electron beam leading to the reduction of gold(IV) ions to metallic gold nanoparticles. To load pocket and crease cells, a droplet of 10×10^{-3} M solution of $HAuCl_4$ was placed on the TEM grid prior to transfer of the graphene top layer by the LAT method. The formation of Au nanoparticles from $HAuCl_4$ solution was chosen as a test reaction because it is a well-documented procedure that has been extensively characterized in literature.[29,30] After 10 s of beam exposure, nanoparticles of varying sizes had formed in all liquid cells, with high contrast regions being, indeed, pockets of encapsulated liquid (**Figure 4**a–c). Elemental mapping by energy-dispersive X-ray spectroscopy confirmed that the observed growing features were indeed gold nanoparticles (Figure S6, Supporting Information).

Remarkably, the loading of fold cells did not require the transfer of a graphene top layer. The aqueous solution of $HAuCl_4$ was flushed underneath the polymer film-support graphene layer after Step II in Figure 1a. The polymer-graphene stack was then scooped onto the TEM grid from the liquid surface, encapsulating the $HAuCl_4$ solution in fold cells, as is evident from gold nanoparticle formation (Figure 4d–f). The formation and loading of graphene liquid cells from a single layer of graphene is an important observation because to date, graphene liquid cells have always required the assembly of two graphene layers.

2.4. GLCs under the Electron Beam

Under the electron beam, graphene liquid cells undergo bubble formation. In Figure 3b, a number of cells have a low contrast region at their center where liquid water has receded. The appearance of a bubble is due to water splitting by radiolysis.[31] When hydrogen concentration in the liquid reaches a critical value, instantaneous bubble formation ensues. As the formation of a bubble inside the liquid cell increases the pressure on the cell walls, the development of a bubble in GLCs is related to the stability of the seal formed by graphene. Next, we discuss the stability of the different cell types in terms of the observed bubble formation under relatively strong beam exposure.

Figure 5a–c show selected frames of a fold cell under a beam exposure of 144 $e^{-}Å^{-2}s^{-1}$ accelerated to 120 keV. (Typically ≈10 $e^{-}Å^{-2}$ s^{-1} at 1–2 s exposure time is used for high resolution imaging of single particles). Already on the first frame a region of light contrast, i.e., a bubble, has appeared. During live observation of many liquid cells, we observed that

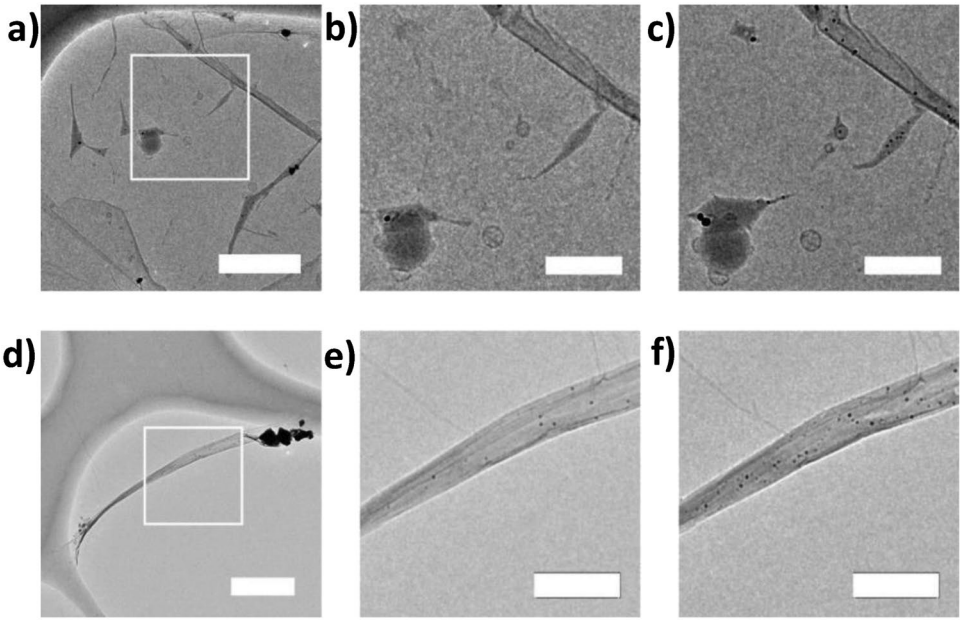

Figure 4. Gold nanoparticle formation in three cell types imaged by TEM. a) Fold cell encapsulating $HAuCl_4$ solution at the start of beam exposure. Scale bar: 500 nm. b) Zoomed-in area of the red square in a). A few nanoparticles have already formed during initial beam exposure. Scale bar: 200 nm. c) The same area after 10 s of beam exposure of ~100 $e^- Å^{-2} s^{-1}$, during which Au nanoparticles have developed in the liquid phase. Scale bar: 200 nm. d) Crease and pocket cells encapsulating $AuCl_3$ solution. Scale bar: 500 nm. e) Zoomed-in area of the red square in (d). Scale bar: 200 nm. f) Same area as in (e) after 4 s of beam exposure. Scale bar: 200 nm.

liquid cells generally contain no bubble during the first moment of beam exposure, but under the strong beam conditions used bubble formation was too rapid to capture a bubble-free GLC. From the first frame on, the bubble moves around the available space in the liquid cell, until the content disappears completely. This may be understood as liquid escaping into vacuum due to the damage induced by the electron beam to the graphene layer.

Figure 5d–f shows selected frames from a pocket cell. Again, a bubble has formed during the first instance of electron exposure. However, unlike the fold cell, dark contrast remains present in the pocket cell even after extended exposure to a relatively strong electron beam. For a bubble to nucleate and form an equilibrium with remaining liquid water, evidently the sealing between the two graphene layers around pocket cells results in very leak-resistant encapsulation. In Figure 3b, various pocket cells have undergone bubble formation whereas others retain uniform dark contrast after prolonged beam exposure. This was a general trend observed in all pocket cells. Figure 5g graphs the percentage of pocket cells that did show collapse under beam exposure, revealing a strong correlation to the number of corners—and thus the curvature of cells. A possible explanation is that, in few-cornered cells, the close-to-flat graphene layers do not allow for the increase in volume required for bubble formation and the GLC is extremely stable.

Over all, the stability and leak-resistance of pocket cells makes them favorable candidates for future applications. Fold cells are evidently more weakly sealed than pocket cells. Even so, the larger volume and unmistakable dynamic liquid content lend themselves very well to encapsulation of larger, macromolecular specimen. Moreover, the ease of fabricating the single graphene layer required to form fold cells is an obvious advantage.

3. Conclusion

The preparation of graphene liquid cells requires large sheets of intact single layer graphene to be transferred without supporting layers. We have presented a reproducible approach that yields millimeter large single layer graphene sheets onto a TEM grid. As liquid cell formation occurs randomly over the grid, we introduced correlated fluorescent light-electron microscopy to locate fluorescent dye-tagged GLCs on the grid prior to exposure to the electron beam. Three types of graphene liquid cells form under a flexible graphene top layer, each with typical size distribution and stability. We showed that the morphology of the seam between the two graphene layers is a determining factor in the stability of encapsulation. In particular, fold type cells form in places where a ruptured graphene sheet curls up, capturing water. Because of this formation process, only a single layer of graphene is required and these cells have a larger probability of encapsulating a larger volume of liquid. Dominating the size range between 250 and 400 nm, fold cells are suitable for encapsulating macromolecular assemblies in the development of GLCs for real-time imaging of liquid-phase biological systems. The demonstration of CLEM, in particular, allows the development of protocols for automated data-collection, targeting the positions on the grid that were identified by fluorescence for electron image recording. Not only will this prevent beam damage prior to imaging, it will also open up the possibility of automated data collection on liquid-phase samples and to recording tomography images as

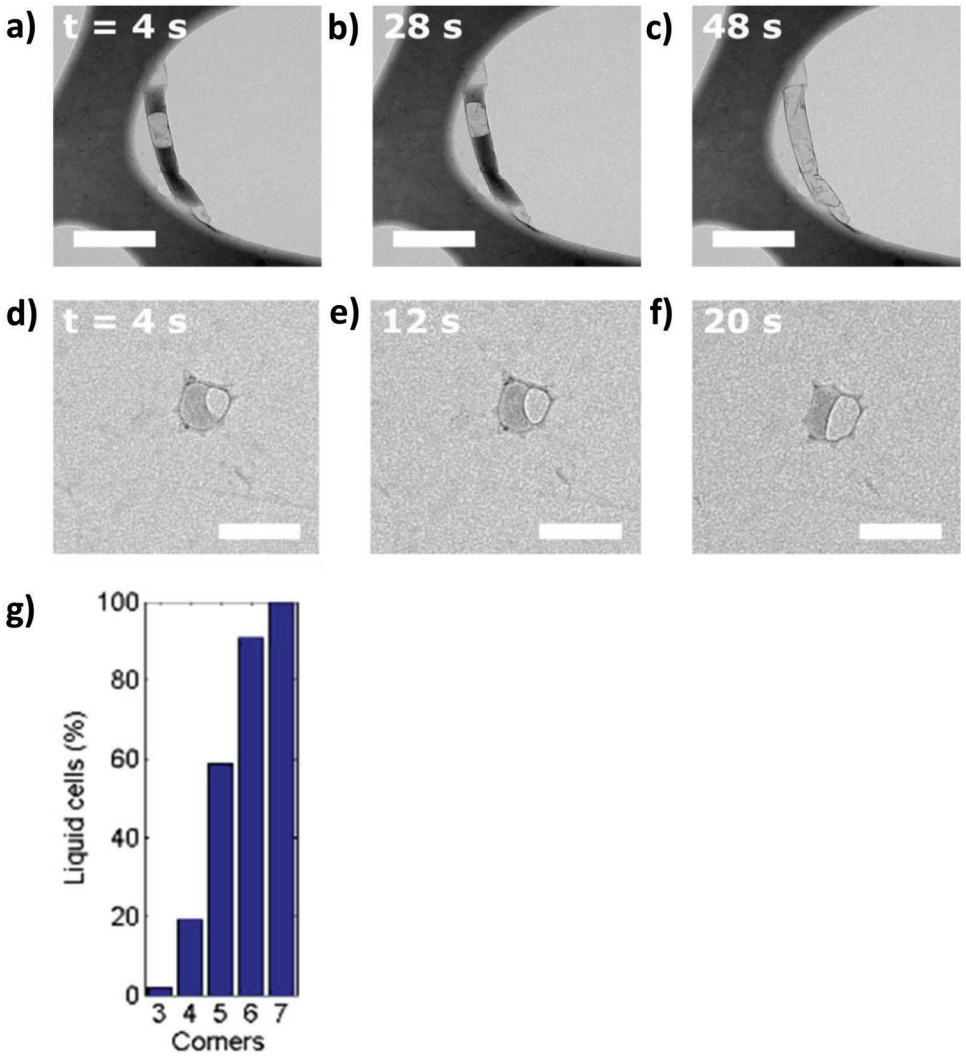

Figure 5. Bubble formation in fold and pocket cells imaged by TEM. a–c) Bubble formation and expansion in a pocket cell. Within the first second of irradiation a bubble appears that grows under prolonged beam exposure. Scale bar: 500 nm; d–f) bubble formation and movement in a fold cell, followed by cell collapse. Scale bar: 100 nm; g) percentage of pocket cells where the onset of bubble formation was observed, correlated to the number of corners in the circumference of the cell. The number of corners is a measure of the curvature of the graphene top layer.

are currently widely used to generate 3D reconstruction of cryogenic samples.

4. Experimental Section

Preparation and Handling of Graphene for GLC Fabrication: Graphene was grown onto copper foil by chemical vapor deposition in a PlanarGrow-2S tube oven (Planar Tech). Raman spectra and electron diffraction patterns are provided in Figure S1 (Supporting Information). To obtain a copper foil featuring graphene on only one side of the foil, one side of the copper foil was protected by a glass slide taped around the etches of the copper foil. Graphene on the other side was then exposed to oxygen plasma (2 min, 160 Watt), rendering a copper foil with a single graphene layer.

Porous polymer support films were made from a solution of 0.5% polystyrene (average M_w ≈192.000, Merck) in ethyl acetate (Merck). Ten volume-percent of glycerol (≥99.0%, Merck) was added to form a biphasic mixture. Shaking the mixture thoroughly for 1 min created a dispersion of glycerol in polystyrene solution. The duration of shaking governs the size and density of pores in the film. A glass slide was then dipped in the dispersion and lifted out, forming a porous polystyrene film on the glass surface. The film was cleaned away from one side of the glass slide. The remaining film on the other side was then lifted off from the glass slide by slowly dipping the glass slide into ultrapure water,[32] rendering the polystyrene film floating on water. Polystyrene porous films prepared from a 0.5% polystyrene solution have a thickness of 30 ± 5 nm, as confirmed by atomic force microscopy on the film deposited on a silicon wafer.

Graphene on copper was cut out in 3 mm circles. The pieces were placed onto the polymer film on water, so that the graphene side interfaced with the polymer film. The pieces were then picked up from the surface of water, while the polystyrene film adhered to the graphene-copper flake. After drying in air, the pieces were placed copper-face down on a 0.1 M aqueous solution of ammonium persulfate (APS, ≥98%, Merck) to etch copper. When copper was removed, the APS solution was replaced with ultrapure water by slow pumping to prevent surface vibration that might damage the graphene layer. The graphene-polystyrene stacks were then scooped onto a gold TEM grid (rendered hydrophilic by 2 min oxygen plasma exposure), resulting in porous polystyrene-supported graphene TEM substrates.

To form liquid cells, a second layer of graphene was transferred onto the graphene-polystyrene covered TEM substrates. To obtain the free-floating graphene ready for transfer, 3 mm diameter pieces of graphene-on-copper were placed onto the surface of 0.1 M APS etching solution. A floating plastic frame with a round hole was used to stabilize the graphene during copper etching. Overnight etching at 4 °C resulted in dissolution of copper. APS solution was then replaced with ultrapure water by slow pumping, after which the graphene was transferred onto the TEM grid substrate using one of the transfer methods described in the main text.

Graphene Liquid Cell Count: To obtain a representative count of GLCs on grids fabricated via the three transfer methods (grid sandwich method, touch-down method and LAT), grids were screened using transmission electron microscopy. On grids with high GLC density (>1 GLC per grid square of $100 \times 100\ \mu m^2$) at least eight grids squares were inspected to obtain an estimate of the GLC density. On grids were the liquid cell density was low (<1 GLC per grid square of $100 \times 100\ \mu m^2$) a larger area was inspected to obtain a reliable estimate of the GLC density.

For the grid-sandwich method, graphene on Quantifoil support film (supplied by Van Loenen Instruments the Netherlands) was used because a flat surface is required for GLC formation to succeed. Out of twenty attempts, six grid-sandwiches were successfully assembled (30%). Failed attempts were typically due to misalignment of the two grids at the moment the two grids made contact. Misaligned stacks were unusable as they do not fit in the sample holder of the electron microscope. Of the six successful stacks, liquid cells were found on only one (≈15%). The overall liquid cell count over these six grids was three, and these cells were partially or completely located on the carbon support film, not on free-standing graphene.

For the touch-down method, top-layer graphene deposition was successful on eight out of twelve attempts (66%). Failure was typically due to graphene drifting away from the grid the moment the grid was touched down, with the graphene sheet breaking into pieces or crumbling so that the attempt at deposition could not be repeated. During inspection of the eight grids, GLCs were found on two grids (25%), with a total of eighteen observed liquid cells on these two grids.

For the LAT method, twenty-one out of twenty-four attempted graphene depositions were successful (88%). Failure was typically due to collapse of the water droplet in the loop. Of the twenty-one grids, GLCs were observed on nineteen grids (90%). The total GLC count was 184 on these twenty-one grids.

Fluorescent Light Microscopy: Fluorescent labeling of GLCs was achieved by depositing a 10 droplet of a 10×10^{-3} M aqueous solution of Atto 488 fluorescent dye (≥98%, Merck) onto the TEM grid coated with graphene and the porous support polymer. The top graphene layer was then deposited via the loop-assisted transfer method, allowing the dye solution to mix with the ≈2 µL droplet of ultrapure water carrying graphene in the loop. Fluorescent light microscopy was performed on a Zeiss Axio Image M2 equipped with a Linkam CMS196M cryo stage. The correlation to electron microscopy was done using MAPS software (Thermo-Fisher Scientific).

Electron Microscopy: GLC TEM grids were prepared within 48 h before insertion in the electron microscope. The collection of cell size statistics was performed using a JEOL 1010 microscope operating at 100 kV. Low-dose high-resolution imaging of single liquid cells was performed on a Tecnai F20 microscope (Thermo-Fisher Scientific, formerly FEI) equipped with a field emission gun as electron source, operated at an acceleration voltage of 200 kV to minimize interaction of the beam with the sample.[33] Electron images were recorded with a Gatan US 4000 camera.

Supporting Information

Supporting Information is available from the Wiley Online Library or from the author.

Acknowledgements

P.M.G.D. and G.F.S. acknowledge the funding received for this work through the European Research Commission (ERC) Starting Grant and the VIDI Innovational Research Incentives Scheme from the Netherlands Organisation for Scientific Research (NWO). A.J.K. was partly supported by the NWO domain Applied and Engineering Sciences (Stichting Technologische Wetenschappen, STW) Perspectief Grant Microscopy Valley, STW12713. A.J.K. and R.I.K. were partly supported by iNEXT, project number 653706, and by the NWO-STW project number STW13711. J.P.P. was supported by the Marie Sklodowska-Curie Action project "LPEMM." M.-A.M was supported by the 4TU.High-Tech Materials research program "New Horizons in designer materials."

Conflict of Interest

The authors declare no conflict of interest.

Keywords

correlated light-electron microscopy, graphene liquid cells, graphene transfer., liquid phase electron microscopy, time-resolved electron microscopy

Received: June 3, 2019
Revised: November 11, 2019
Published online: February 3, 2020

[1] J. M. Yuk, J. Park, P. Ercius, K. Kim, D. J. Hellebusch, M. F. Crommie, J. Y. Lee, A. Zettl, A. P. Alivisatos, *Science* **2012**, *336*, 61.
[2] Q. Chen, J. M. Smith, J. Park, K. Kim, D. Ho, H. I. Rasool, A. Zettl, A. P. Alivisatos, *Nano Lett.* **2013**, *13*, 4556.
[3] J. M. Yuk, Q. Zhou, J. Chang, P. Ercius, A. P. Alivisatos, A. Zettl, *ACS Nano* **2016**, *10*, 88.
[4] N. D. Loh, S. Sen, M. Bosman, S. F. Tan, J. Zhong, C. A. Nijhuis, *Nat. Chem.* **2017**, *9*, 77.
[5] X. Ye, M. R. Jones, L. B. Frechette, Q. Chen, S. C. Nguyen, V. P. Adiga, A. Zettl, E. Rabani, *Science* **2016**, *354*, 874.
[6] J. Y. Cheong, J. H. Chang, H. K. Seo, J. M. Yuk, J. W. Shin, J. Y. Lee, I. D. Kim, *Nano Energy* **2016**, *25*, 154.
[7] J. J. De Yoreo, N. A. J. M. Sommerdijk, *Nat. Rev. Mater.* **2016**, *35*, 1.
[8] A. Ianiro, H. Wu, M. M. J. Van Rijt, M. P. Vena, A. D. A. Keizer, A. C. C. Esteves, R. Tuinier, H. Friedrich, N. A. J. M. Sommerdijk, J. P. Patterson, *Nat. Chem.* **2019**, *11*, 320.
[9] Z. S. S. Pohlmann, K. Patel, S. Guo, M. J. Dukes, D. F. Kelly, *Nano Lett.15*, **2015**, 2329.
[10] N. de Jonge, *Ultramicroscopy* **2018**, *187*, 113.
[11] H. Cho, M. R. Jones, S. C. Nguyen, M. R. Hauwiller, A. Zettl, A. P. Alivisatos, *Nano Lett.* **2017**, *17*, 414.
[12] N. De Jonge, L. Houben, R. E. Dunin-Borkowski, F. M. Ross, *Nat. Rev. Mater.* **2019**, *4*, 61.
[13] S. Keskin, N. de Jonge, *Nano Lett.* **2018**, *18*, 7435.
[14] J. Park, H. Park, P. Ercius, A. F. Pegoraro, C. Xu, J. W. Kim, S. H. Han, D. A. Weitz, *Nano Lett.* **2015**, *15*, 4737.
[15] I. N. Dahmke, A. Verch, J. Hermannsdörfer, D. B. Peckys, R. S. Weatherup, S. Hofmann, N. De Jonge, *ACS Nano* **2017**, *11*, 11108.
[16] K. H. Nagamanasa, H. Wang, S. Granick, *Adv. Mater.* **2017**, *29*, 1703555.

[17] Y. C. Lin, C. C. Lu, C. H. Yeh, C. Jin, K. Suenaga, P. W. Chiu, *Nano Lett.* **2012**, *12*, 414.
[18] M. Textor, N. De Jonge, *Nano Lett.* **2018**, *18*, 3313.
[19] J. Zhang, L. Lin, L. Sun, Y. Huang, A. L. Koh, W. Dang, J. Yin, M. Wang, C. Tan, T. Li, Z. Tan, Z. Liu, H. Peng, *Adv. Mater.* **2017**, *29*, 1.
[20] E. Firlar, M. Ouy, A. Bogdanowicz, L. Covnot, *Nanoscale* **2019**, *11*, 698.
[21] A. P. A. Matthew, R. Hauwiller, J. C. Ondry, *J. Visualized Exp.* **2018**, *135*, e57665.
[22] J. Yang, S. B. Alam, L. Yu, E. Chan, H. Zheng, *Micron* **2019**, *116*, 22.
[23] E. Firlar, M. Ouy, L. Covnot, D. Lee, A. Chan, S. Afelik, Y. Wang, *Int. J. Nanomed.* **2019**, *14*, 371.
[24] Y. Sasaki, R. Kitaura, J. M. Yuk, A. Zettl, H. Shinohara, *Chem. Phys. Lett.* **2016**, *650*, 107.
[25] D. J. Kelly, M. Zhou, N. Clark, M. J. Hamer, E. A. Lewis, A. M. Rakowski, S. J. Haigh, R. V Gorbachev, *Nano Lett.* **2018**, *18*, 1168.
[26] A. Boscá, J. Pedrós, J. Martínez, T. Palacios, F. Calle, *Sci. Rep.* **2016**, *6*, 21676.
[27] W. Regan, N. Alem, B. Alemán, B. Geng, L. Maserati, F. Wang, M. Crommie, A. Zettl, *Appl. Phys. Lett.* **2010**, *96*, 113102.
[28] E. Khestanova, L. Fumagalli, A. K. Geim, I. V Grigorieva, *Nat. Commun.* **2016**, *7*, 12587.
[29] C. Zhu, S. Liang, E. Song, Y. Zhou, W. Wang, F. Shan, Y. Shi, C. Hao, K. Yin, T. Zhang, J. Liu, H. Zheng, L. Sun, *Nat. Commun.* **2018**, *9*, 421.
[30] Y. Zhang, D. Keller, M. D. Rossell, R. Erni, *Chem. Mater.* **2017**, *29*, 10518.
[31] J. M. Grogan, N. M. Schneider, F. M. Ross, H. H. Bau, *Nano Lett.* **2014**, *14*, 359.
[32] G. F. Schneider, V. E. Calado, H. Zandbergen, L. M. K. Vandersypen, C. Dekker, *Nano Lett.* **2010**, *10*, 1912.
[33] R. F. Egerton, *Ultramicroscopy* **2014**, *145*, 85.